Simulations in the Development of the Barrel Muon Chambers for the CMS Detector at LHC

A. Benvenuti [b], J. Berdugo [c], S. Bethke [a], M. Cerrada [c], N. Colino [c], B. Fehr [a], F. Gasparini [d], V. Giordano [b], P. Guaita [d], P. Ladrón de Guevara [c], S. Marcellini [b], A. Meneguzzo [d], J. Mocholí [c], F.L. Navarria [b], M. Pegoraro [d], H. Reithler [a], L. Romero [c], P. Ronchese [d], T. Rovelli [b], P. Sartori [d], H. Schwarthoff [a], L. Stanco [d], V. Tano [b,1], H. Teykal [a], E. Torassa [d], J. Tutas [a], H. Wagner [a] and P. Zotto [d]

[a] *III. Physikalisches Institut A, RWTH Aachen, D-52056 Aachen, Germany*

[b] *I.N.F.N. Sezione di Bologna and Dipartimento di Fisica Università di Bologna Via Irnerio 46, I-40126 Bologna, Italy*

[c] *CIEMAT - Divison de Fisica de Particulas, Avenida Complutense 22, E-28040 Madrid, Spain*

[d] *I.N.F.N. Sezione di Padova and Dipartimento di Fisica Università di Padova, Via Marzolo 8, I-35131 Padova, Italy*

Abstract

The development of the barrel drift chambers for the CMS muon detector at the CERN *Large Hadron Collider* is supported by a variety of simulation calculations, based on the GARFIELD drift chamber simulation program and the GEANT detector simulation package. This study surveys the results influencing the actual chamber design. The dependence of the drift cell performance on shape and position of the cell electrodes as well as on the mechanical tolerances is shown. The results obtained for space-time relation and spatial resolution are in good agreement to test beam measurements on prototypes.

[1] now at RWTH Aachen

Preprint submitted to Elsevier Preprint *18 July 1997*

1 Introduction

The barrel drift chamber being developed for the muon detector of the CMS experiment at the Large Hadron Collider ([1], [2]) at CERN is a conventional drift chamber with a 40 mm×13 mm cell, operating at athmospheric pressure and room temperature [2]. Since the collisions of protons within LHC take place every 25 ns, which is much smaller than the maximum drift time of 340 ns, it is important to determine the originating bunch crossing for every measurement. The chamber modules have a length of 2.5 m and a width varying from 2 m to ca. 4 m. Each chamber consists of three groups of 4 drift tube layers. Two of them measure the particle deflection in the magnetic solenoidal field. They are separated by a honeycomb spacer of ca. 13 cm and the third group, measuring the track component along the particle beam. The cells of consecutive layers are staggered by half a cell width to enable resolution of left-right ambiguities. This also allows to generate a signal which gives the time of particle crossing t_0 and thus the bunch crossing: one uses the fact that for three consecutively hit cells the drift distance of the second cell and the mean value of the other two sum to half the cell width. A similar expression holds for the drift times, as far as the space-time relation is linear.

The cross sections of two considered options of the drift cell are shown in figure 1. The first design is a rectangular cell with a centered anode wire and I-shaped aluminium cathode profiles as cell walls, where grounded aluminium plates make up the chamber plane. In the second design one further potential is added by two insulated strip electrodes, glued onto the ground plates. The cathodes are insulated towards the plates by plastic profiles with a shape optimized for high voltage stability.

Unless specified otherwise all computations and measurements have been performed using the standard drift gas: 85 % Argon/15 % CO_2.

The physical processes that are important for the generation of a drift chamber signal are described in detail by the program GARFIELD ([4]). It features the computation of drift times and their distributions, including effects from primary ionisation in the drift gas, drift and diffusion properties and the development of a chamber pulse (i.e. the avalanche at the anode wire). The data for the drift gas properties are delivered by the GARFIELD-interfaced program MAGBOLTZ ([6]): drift velocity, diffusion coefficients and townsend coefficients for computation of gas gain. The detector simulation program GEANT ([9]) has been used for the description of the chamber body and the generation of particle tracks crossing the chamber.

In order to gain confidence in the simulation results it is important to compare

[2] The general concept has been described in [3],[8].

them to measured data. The GARFIELD online documentation ([7]) mentions such comparisons for drift velocity and gas gain, showing that the drift velocity is reproduced well by the calculations, while the gas gain can only be considered accurate within two orders of magnitude. A direct comparison for the drift velocity with the gas used in the work described here is given in [8]. Checks of the simulation model and of the computed gas data are presented in the following sections.

2 Space-time relation

The mean space-time relation t(x), describing the drift time t for a particle crossing the drift cell at a distance x from the anode wire (accounting only for drift velocity, cell geometry and electric field) depends on the incidence angle of the particle and can be calculated directly by GARFIELD. This leads to the possibility of optimizing the cell design following the desired guidelines:

- Linearity of space-time relation within ca. 4 ns ([10])
- Mechanical stability of the chamber
- Low cost
- Low sensitivity of the chamber to mechanical tolerances
- Small dead space at chamber borders

The described studies have been carried out assuming an incidence angle of 0^o (i.e. normal to the chamber plane), unless it is stated otherwise.

2.1 Linearity of space-time relation

It is desirable to have a space-time relation that is as linear as possible, because the first level muon trigger is then capable of generating a bunch crossing signal for a track segment in a muon chamber. The system foreseen for this task has been described in [10].

Figure 2 shows the deviation of the space-time relation from a straight fit line for different widths of the cathode profile and for the simple cell type with an optimized cathode width of 13 mm. The coordinate system used here is sketched in the figure; the origin is defined to be the anode wire location. The third coordinate, z, is parallel to the anode wire. Unless stated otherwise, the direction of particle incidence is parallel to the y axis.

The drop of the electric field (and consequently of the drift velocity) in the cathode region worsens for wider cathodes, causing non-linearities of up to 0.7 ns in the case of the 11 mm cathode. The simple cell type shows deviations of 3 ns. The real constraints come from the working conditions in magnetic field (see section 2.2), because there the induced non-linearities are much larger.

A similar study has been carried out for the additional strip electrode, revealing that its width should be around 15 mm, however without strong constraints.

2.2 Magnetic field

In order to attain simulation results for drift cells in magnetic field of a similar quality as those described above, a particular treatment of the drift processes is needed. The considerable progress in the recent GARFIELD development introduced generation of proper gas data: the drift velocity and diffusion coefficients depend on the strength *and* on the orientation of the magnetic field, resulting in accurate computation of the Lorentz angles (a comparison of calculation to experimental data is quoted in [7]).

The highest challenge of the linearity of space-time relation is encountered in those muon chambers which are close to the end of the magnet coil, where the magnetic field has its main component perpendicular to the chamber plane and varies between zero and 0.9 T along the 2.55 m long anode wires. The chamber trigger has to use a space-time relation suitable for the whole range of magnetic field. Some cells near the chamber edges are lying in another critical, but small region, with fields of up to 0.4 T, oriented parallel to the anode wires which measure the muon momentum.

Figure 3 shows the linearity of the space-time relation for the two critical field conditions in cells with three different cathode profile widths (a) and for the simple cell type (b). Notation is $B_{\perp}$ for the field in y direction and $B_{||}$ for the orientation parallel to the wires, i.e. in z direction. The direction of the third field component is parallel to the x axis, i.e. mostly parallel to the movement of the drifting electrons; therefor it does not influence significantly the cell behaviour. The ordinate of the plot is the difference between the space-time relation with magnetic field and the fitted straight line for zero field. It becomes clear that the demands on linearity ([10]) must be applied here, evaluating the performance in magnetic field: the bunch crossing assignment efficiency of the trigger hardware drops dramatically, if the average drift velocity differs from the foreseen value by more than ca. 1–2%. Figure 3 shows that this condition is violated at the extremes of the magnetic field. The effect is much stronger for the simple cell.

A magnetic field of up to $B_{||} = 0.4$ T, also shown in figure 3, gives high deviations near the cathode, but can be limited by choosing a small cathode width (in the cell with additional electrode). However, another boundary condition limits the cathode width to be not smaller than 7 mm: the mechanical stability of the whole chamber block requires a sufficiently large glueing area between cathode profiles, insulators and ground planes. The fact that the deviations of space-time relation for the simple cell type are much higher lead to the decision to include the additional electrode into the final chamber design. Thus, the following studies have been carried out for the final cell type only.

2.3 Mechanical tolerances

Calculation of space-time relations for 'non-perfect' cells can give valuable information about the mechanical tolerances valid for the drift chamber construction.

Figure 4 shows the deviation of the space-time relation from the curve for an ideal cell, in a cell with an (unintended) shift of the strip electrode position in x direction. The deviations for the case shown (one strip displaced) are larger than those for displacement of both strips in the same direction. Up to 0.5 mm error can easily be tolerated; also 1 mm gives deviations well below the time resolution of the chamber (which is about 4 ns). From the technical view the assembly of the components in the chamber production can work fine within those values.

The other possible cases, namely positioning errors for the cathode, for the strip electrode (in y direction), and for the anode wire have been studied and turn out to be even less critical in terms of space-time relation (deviations below 0.2 ns for errors of 0.5 mm).

2.4 Border cells

Since adjacent layers are staggered by half a cell width, each layer would lose at least one half cell as sensitive volume at one end. To be able to have also this part operating, a metal closure profile could be placed near the natural 0 V line in the border cell (figure 5 a). This should ensure that the distortions of the space-time relation in the other half of the cell are marginal. The results of the simulation have shown that this is given even within a range of operating voltages and closure profile positions (figure 5 b).

3 Gas multiplication factors

3.1 Simulation parameters

The Garfield simulation is carried out by a superposition of single wire solutions of the Poisson equation ([4]). Thus, complicated cell structures have to be approximated by a number of wires with the corresponding potentials. The resulting accuracy can be estimated by varying diameter of and distance between the wires building up the drift cell.

How much the calculated electric field deviates from reality becomes more clear in figure 6. It shows the calculated field along a straight line in y direction, going from the anode wire to the strip electrode; the end point is chosen to be at the surface of the strip simulating wire (case 1) or in the space between this wire and its neighbour (case 2). In the anode region deviations of up to 15 % are possible, varying the distance between the strip-simulating wires from 20 μm to 100 μm. Due to the subdivision of the strip electrode into individual wires, artificial spikes appear near the electrode (figure 6 b). They are higher for case 2, because here the proximity of the grounded plane has a larger influence.

The diameter of the strip wires was chosen to be slightly (1 μm) smaller than the distance between their centers. Using lower values (thus having larger spacing between the wires) leads to higher spikes, so moving the simulation further away from reality.

The space-time relation is unaffected by the field deformations shown in figure 6, because the drift velocity does not change significantly with field in the relevant range, which is the region near the x axis. The quantity which depends strongly on the simulation is the gas gain, also computable with GARFIELD. The simulation integrates the *Townsend coefficient*, i.e. the mean number of avalanche electrons per unit length generated in an electric field, along the drift line. The integration can be confined to the region of less than 1 mm around the anode, because only here (i.e. in electric fields above 10 kV/cm) the coefficient differs from zero.

Figure 7 shows the gas gain at the anode wire computed with GARFIELD versus distance between the wires that simulate the electrode. The fit line is an exponential curve that gives an extrapolated value of 51400 for zero distance. Measurements from one of the prototypes (see below) yielded 41000 ([5]), which is a reasonable agreement.

All calculations presented here have been made using the cell representation shown in figure 5 a. It is possible to reduce the sensitivity of the results on the wire structure of the strip electrode: calculations using a cell description like it is given in figure 8 ([13]) are not sensitive to the diameter and distance of the strip electrode wires, since there is no aluminium plane at a small distance behind the strip. The insulator structures also visible in figure 5 have been placed in the cell as a consequence of a — still ongoing — study of the behaviour of the plastic materials. This study is expected to give an answer to the question, how much the cell function is influenced by the presence of insulators in the cell.

3.2 Tolerances in view of gas gain

Although the conditions of electric field in the region very close to the anode do scarcely influence the space-time relation, the mechanical tolerances of the strip electrode may nevertheless affect the gas gain.

Figure 9 confirms that the dependence of the gas gain from errors in positioning of anode wire, strip electrode, ground plane (i.e. insulator thickness) and cathodes is very small (the fluctuation of individual chamber pulse heights is much larger). However, the validity of these results has to be verified carefully, because using too large values of diameter and distance between the wires that simulate the strip electrode (98 μm and 100 μm, respectively) leads to a larger effect. As an example, the dash-dotted curve in figure 9 shows the result for a y shift of the strip electrode. Only after reducing these values to 19.99 μm and 20 μm, respectively, the effect is small (solid curve).

4 Arrival time distributions

A particle crossing a drift cell looses energy, which leads to the creation of ionisation clusters in the cell gas. The electrons coming from those clusters move along the drift lines towards the anode and are subject to thermal diffusion processes. Thus, the drift time for a particle crossing the cell at a distance x from the anode follows a distribution whose width is a measure for the attainable spatial resolution (for the specified x). We calculated a set of such distributions for ca. 20 x values from zero up to the maximum drift distance and used them in the chamber simulation to obtain a realistic drift time generation.

We verified that transverse diffusion (i.e. diffusion perpendicular to the drift direction) is responsible for a considerable fraction of the drift time spread due to the movement of signal electrons to neighbouring drift lines.

4.1 Detector simulation

The CERN-developed detector simulation package GEANT has been used for the setup of a detailed simulation of a prototype chamber built at Aachen ([8]). It is an assembly of four layers, each with 8 cells, 1 m long, of the cell type described above. Track inclination was achieved by tilting the chamber around the z axis (angle Φ) or around the x axis (angle Θ). Both angles are zero, if the direction of particle incidence is parallel to the y axis. Drift times were determined from the hit locations by using the arrival time distributions mentioned before. Details about the analysis method are given in [11].

4.2 Space-time relation from full analysis

Figure 10 depicts the difference in space-time relation between simulation and experimental data from 300 GeV test beam muons taken at the CERN H2 site in summer 1995. The deviations are $<300\,\mu$m for the standard gas and voltages (dotted curve), but reduce to $<150\,\mu$m, comparing the data to calculations for 14 % CO_2 (solid curve; 300 μm correspond to a time of 5.5 ns with a mean drift velocity of 55 μm/ns). The same effect is observed for a magnetic field of 0.5 T and 1 T and incidence angles between $\Theta = 0$ and $\Theta = 20^o$ (not shown here). Since a de facto CO_2 fraction of 14 % for the chamber gas lies well within the possible variation range of the used mixture it is reasonable to carry out the comparison between data and simulation for this value. Under those circumstances the simulated space-time relations agree within 200 μm with the measurement for all magnetic fields and incidence angles studied over the whole cell width.

The same methods produced similar results for a small-cell drift chamber that has been previously developed in Aachen (WLDC, see [12],[11]).

4.3 Spatial resolution

The detailed statistical simulation and analysis gives space-time relations that look similar to what was shown in section 2. The main difference is the fact that now spatial resolutions can be computed, because the following effects have been added:

- Secondary processes occuring in the chamber (e.g. delta electrons)
- Statistics of primary ionisation in the drift gas
- Diffusion processes in the gas

- Digitization of drift times in steps of 1 ns, to simulate the time measuring device
- Track reconstruction in the analysis software
- Errors in x on anode wire positions following a gaussian distribution with a variance of 100 μm

The geometry of the chamber body, the generation of muon tracks traversing it and the production of secondary particles were described by applying the detector simulation package GEANT. Not included is the effect of signal damping on the anode wire, pulse amplification and shaping in the preamplifier and discrimination to obtain the drift time signal in digital form.

The resulting resolution values are quoted in table 1, together with the measured values, for three different incidence angles Φ. The observed variation of resolution with Φ is well reproduced by the calculations, although it is underestimated by ca. 20 μm for all computed points. This underestimation is probably due to the fact that effects of the readout electronics have been neglected.

Carrying out the simulation process for the magnetic field lead to resolution values that were much too small in comparison to the measurement (e.g. 120 μm compared to 195 μm from measured data), because the treatment of the drift gas properties (especially diffusion) in the presence of magnetic field is still under development in GARFIELD. The calculations of space-time relations, as presented in section 2.2, are not affected by this.

5 Conclusion

Using the drift chamber simulation program GARFIELD and the detector simulation package GEANT a detailed simulation tool for the generation of drift chamber data was set up in order to model the drift chamber behaviour and compare the results to the measurement. Good progress in the development of gas data calculations and treatment of processes taking place in the drift gas have prepared the ground for a realistic simulation.

Studies of space-time relation recommend the cathode width to be chosen as small as possible, since the performance of the bunch crossing assignment poses constraints on the linearity. This is most relevant in the presence of a magnetic field. However, a width below 7 mm can not be realized for reasons of mechanical stability. Construction tolerances for the positions of the strip electrodes and the cathodes come out to be reasonably loose (500 μm) .

Since the gas gain is very sensitive to variations of electric field in the anode region, it depends strongly on the choice of the diameter and distance between the wires that simulate the strip electrode. The space-time relation is hardly influenced by this effect. Extrapolation to the ideal case (infinite number of wires) leads to a gas gain which agrees within 20 % with measurement. Study of this quantity in view of mechanical tolerances also gives a safe 500 μm margin.

The full simulation, including the spread of drift times due to statistical effects, gives a spatial resolution which is about 20 μm below the observation and reproduces the dependence on incidence angle. The reduced values show that still some effects are not properly included in the simulation. However, we expect that the behaviour of the electronics chain is able to account for the difference. Although the drift cell contains small amounts of insulator materials, they were not accounted for in the GARFIELD computations, because preliminary results from a finite element analysis ([13],[5]) showed, that the thin layers of plastics hardly alter the electric field conditions in the drift cell. The final answer to this question will come from a refinement of the detailed simulation, which is currently in progress. Nevertheless the computations have reached a level where they can well be used for overall detector studies.

References

[1] The LHC Study Group: *THE LARGE HADRON COLLIDER, Conceptual Design*, CERN/AC/95-05(LHC), 1995.

[2] CMS Collaboration: *The Compact Muon Solenoid, Technical Proposal*, CERN/LHCC 94-38, 1994.

[3] F. Gasparini et al.: *Performance of a DTBX prototype*, Nucl. Instr. and Meth. in Phys. Res. A 344(1994), p. 137.

[4] R. Veenhof: *Garfield – A drift-chamber simulation program*, CERN program library W5050.

[5] H. Schwarthoff: *Simulationen in Konzeption und Bau der zentralen Myondriftkammern am CMS-Detektor*, Dissertation, RWTH Aachen, 1997.

[6] S. F. Biagi: *A Multiterm Boltzmann Analysis of Drift Velocity, Diffusion, Gain and Magnetic-field Effects in Argon-Methane-Water-Vapour Mixtures*, Nucl. Instr. and Meth. in Phys. Res. A 283(1989), p. 716 is the origin of the MAGBOLTZ program, developed by the same author.

[7] R. Veenhof: *Simulation of 2-dimensional drift chambers*, Online user's guide examples, accessible via *http://consult.cern.ch/writeup/garfield/examples* and the Online user's manual via *http://consult.cern.ch/writeup/garfield/main.html.*

[8] M. Benettoni et al. (CMS barrel muon group): *Performance of the Drift Tubes for the Barrel Muon Chambers of the CMS Detector at LHC*, submitted to Nucl. Instr. and Meth. in Phys. Res..

[9] CERN Application Software Group: *GEANT, Detector Description and Simulation Tool*, Version 3.21, CERN Program library W5013.

[10] M. De Giorgi et al.: *Design and Simulations of the Trigger Electronics for the CMS Muon Barrel Chambers*, CMS Technical Note TN/95-01.

[11] H. Faissner et al.: *Performance of a wall-less drift chamber for muon detection*, Nucl. Instr. and Meth. in Phys. Res. A 356(1995), p. 280.

[12] H. Faissner et al.: *Modular wall-less drift chamber for muon detection at the LHC*, Nucl. Instr. and Meth. in Phys. Res. A 330(1993), p. 76.

[13] T. Rovelli: *Simulation of the CMS Barrel Muon Chambers.* CMS Technical Note TN/95-106.

Figure captions

Figure 1: Cell cross section of the barrel drift tubes for the CMS barrel muon detector. Drift lines reaching the anode and isochrones in 20 ns steps are shown. The upper cell is the primary design, the lower the result of the development considering linearity of space-time relation. The electrode voltages as indicated in the picture are referred to as U = 1.8 kV/-3 kV for the simple cell type and U = 3.3 kV/±1.5 kV for the other.

Figure 2: Deviation of space-time relation from linear behaviour, shown for different cathode profile widths and for the simple cell type. The curve for the simple cell was calculated with U = 1.9/-3 kV; the other refer to U = 3.6/±1.75 kV.

Figure 3: Deviation of space-time relation from a straight line optimized for B = 0. Plot a) shows the computations with additional electrode for different cathode profile widths (U = 3.6/±1.75 kV); in plot b) the simple drift cell has been used (U = 1.9/-3 kV). The two considered magnetic field conditions are given.

Figure 4: Deviation of space-time relation from that of an ideal cell in the presence of errors in horizontal electrode strip positioning. The curves show the left (L) and right (R) sides of the cell, respectively.

Figure 5: a) Equipotential lines in the drift cell. The 0 V line (see arrow) is straight. In this position a closure profile connected to the grounded chamber planes can be placed in the border cell to maintain functioning of the other cell half. b) Deviation of space-time-relation from linearity in the operating half cell, if the proposed closure profile is placed in the other half cell. Two cases of profile positions are indicated.

Figure 6: Electric field along a straight line from anode wire (center at y = 0, surface at y = 25 μm) to one strip electrode (y = 0.54 cm) for different spacings d of the wires that simulate the electrode. a) Anode region, affecting mostly the gas gain. b) Near the strip electrode. The endpoint of the line is chosen to be on the surface of a wire (solid curves, case 1) and in the space between two wires (dashed curves, case 2). The three curves of the same line style, respectively, correspond to d = 100, 50 and 20 μm (from left to right). U = 3.6/±1.75 kV.

Figure 7: Gas gain (a) and electric field (b) at anode wire vs. distance between electrode-simulating wires. The exponential curve fits well the points and gives a gain of 51400 for zero distance; the linearly extrapolated electric field yields 148 kV/cm. The cell parameters are the same as in figure 6.

Figure 8: Alternative representation of the cell structure for the GARFIELD calculations (compared to figures 1 and 5 a). The main difference is the missing aluminium plane behind the strip electrode.

Figure 9: Relative change in gas gain for different 'non-perfect' cells, as indicated. The dash-dotted curve shows up a simulation artifact (see text).

Figure 10: Difference in space-time relation between test beam data and simulation for $\Phi = \Theta = 0$, using the full GEANT/GARFIELD description. The dotted curve shows deviations from zero of up to $300\,\mu$m; the calculation for $14\,\%$ CO_2 instead of $15\,\%$ nominal (solid curve) is much closer to the experiment.

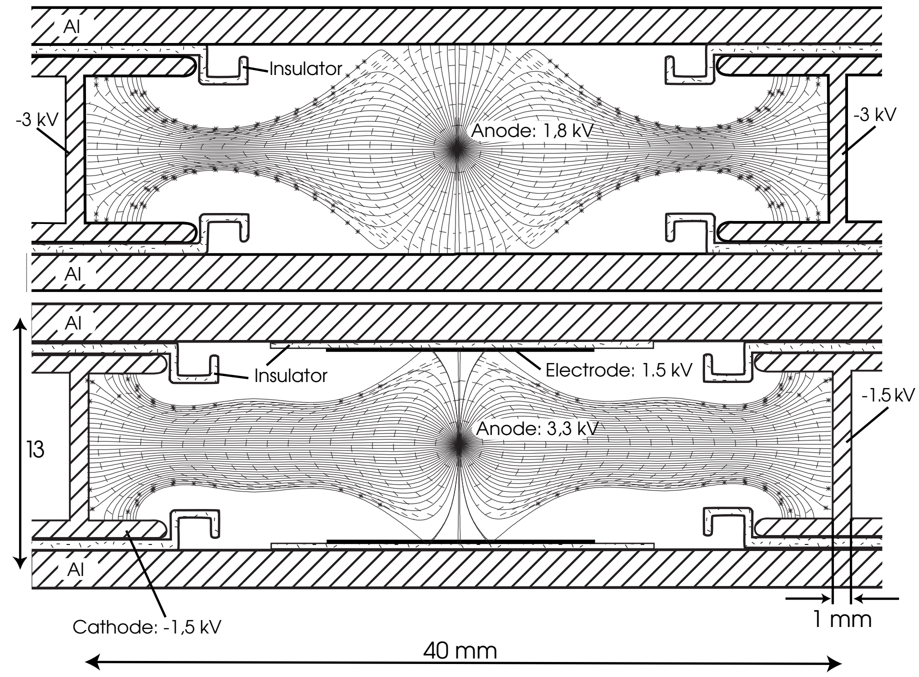

Al
Insulator
-3 kV
Anode: 1,8 kV
-3 kV
Al
Al
Insulator
Electrode: 1.5 kV
-1.5 kV
13
Anode: 3,3 kV
Al
Cathode: -1,5 kV
1 mm
40 mm

Fig. 1.

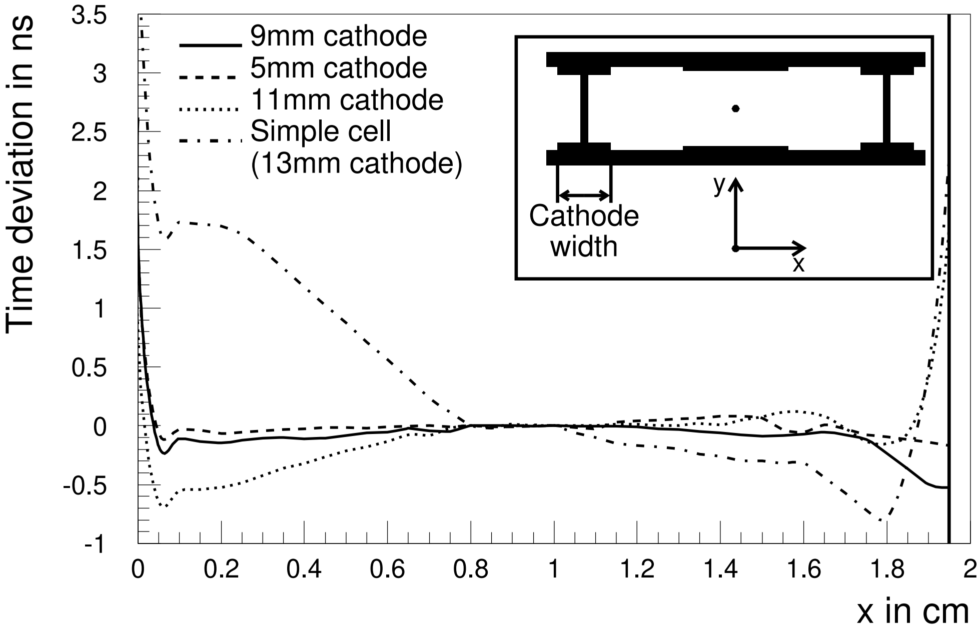

Time deviation in ns
3.5
3
2.5
2
1.5
1
0.5
0
-0.5
-1
0
0.2
0.4
0.6
0.8
1
1.2
1.4
1.6
1.8
2
x in cm
9mm cathode
5mm cathode
11mm cathode
Simple cell
(13mm cathode)
Cathode
width
y
x

Fig. 2.

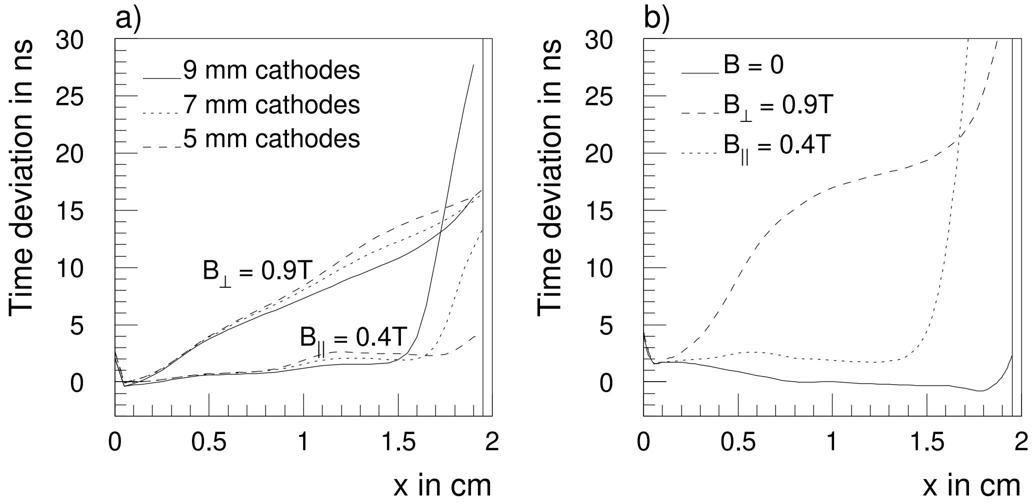
a)
Time deviation in ns
9 mm cathodes
7 mm cathodes
5 mm cathodes
B⊥ = 0.9T
B|| = 0.4T
x in cm
b)
Time deviation in ns
B = 0
B⊥ = 0.9T
B|| = 0.4T
x in cm

Fig. 3.

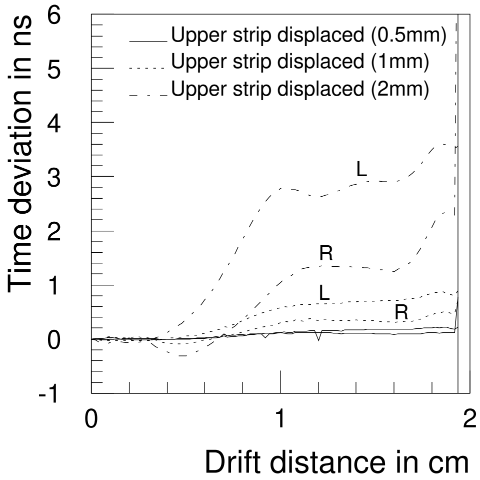
Upper strip displaced (0.5mm)
Upper strip displaced (1mm)
Upper strip displaced (2mm)
L
R
L
R
Time deviation in ns
Drift distance in cm
6
5
4
3
2
1
0
-1
0
1
2

Fig. 4.

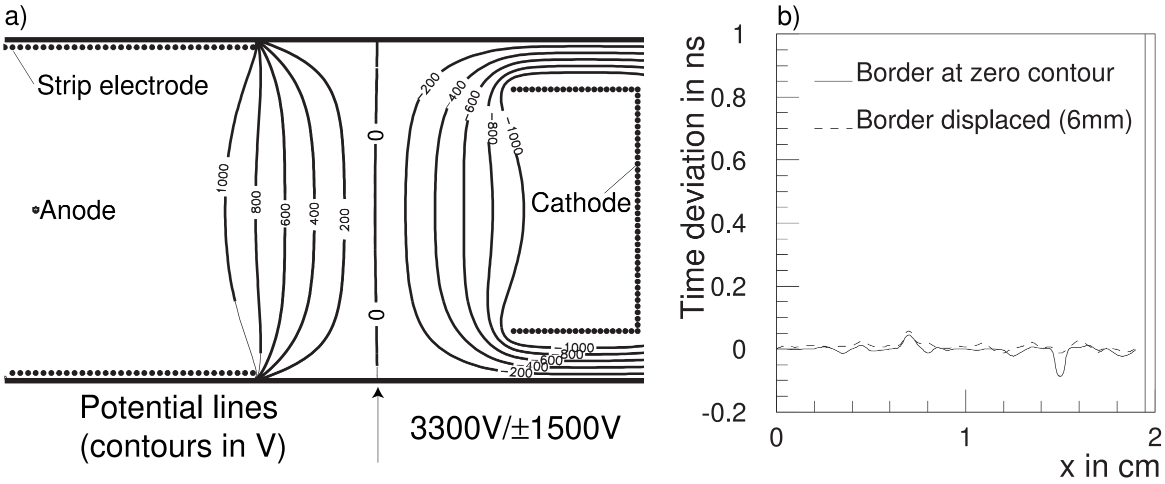
a)
Strip electrode
Anode
Cathode
1000
800
600
400
200
0
-200
-400
-600
-800
-1000
Potential lines
(contours in V)
3300V/±1500V
b)
Time deviation in ns
Border at zero contour
Border displaced (6mm)
1
0.8
0.6
0.4
0.2
0
-0.2
0
1
2
x in cm

Fig. 5.

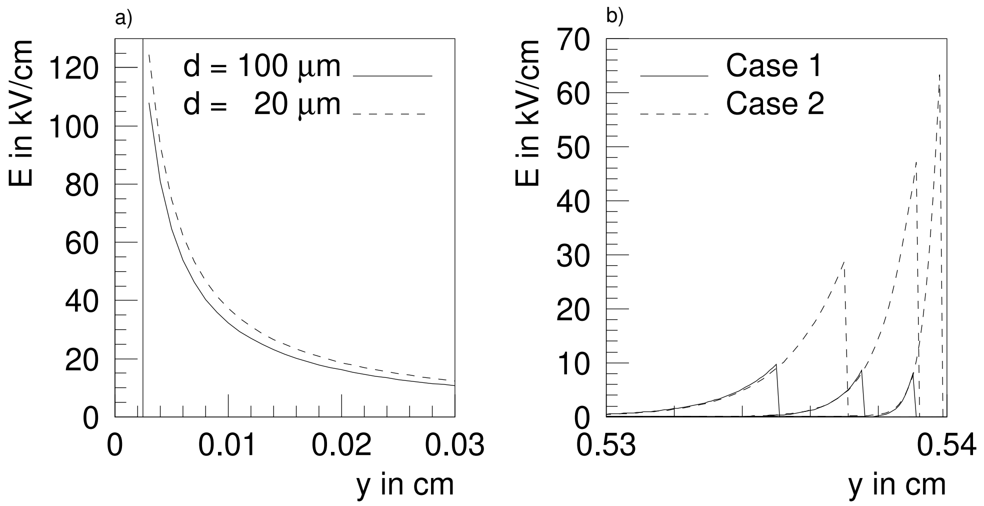
a)
E in kV/cm
120
100
80
60
40
20
0
d = 100 μm
d = 20 μm
0
0.01
0.02
0.03
y in cm
b)
E in kV/cm
70
60
50
40
30
20
10
0
Case 1
Case 2
0.53
0.54
y in cm

Fig. 6.

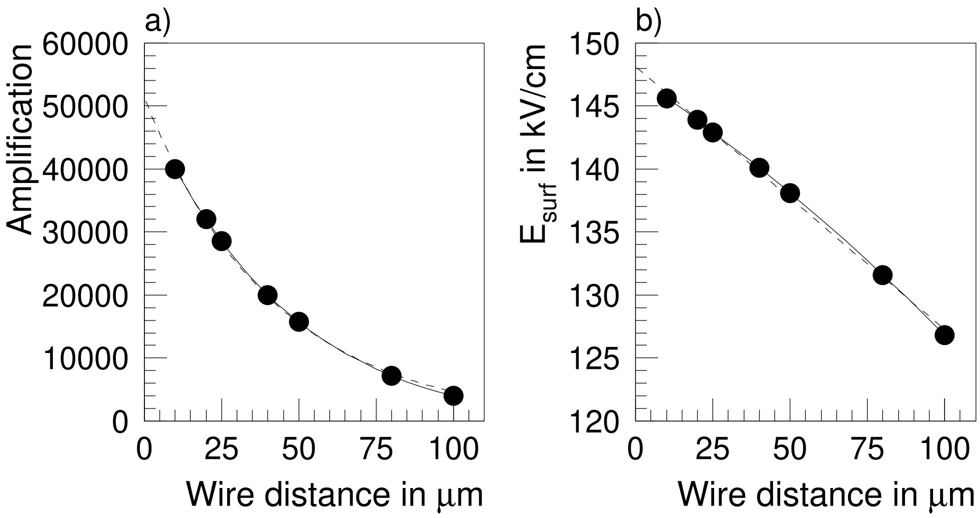
a)
Amplification
60000
50000
40000
30000
20000
10000
0
0
25
50
75
100
Wire distance in μm
b)
E_{surf} in kV/cm
150
145
140
135
130
125
120
0
25
50
75
100
Wire distance in μm

Fig. 7.

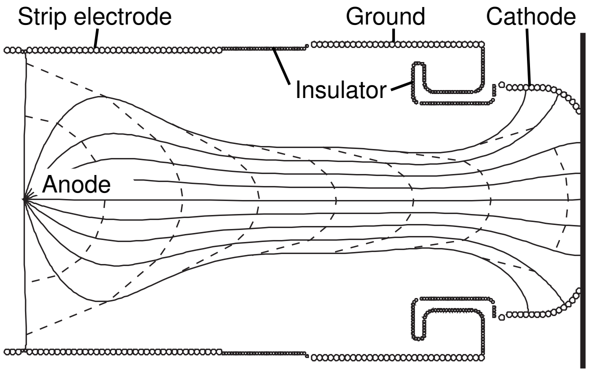

Fig. 8.

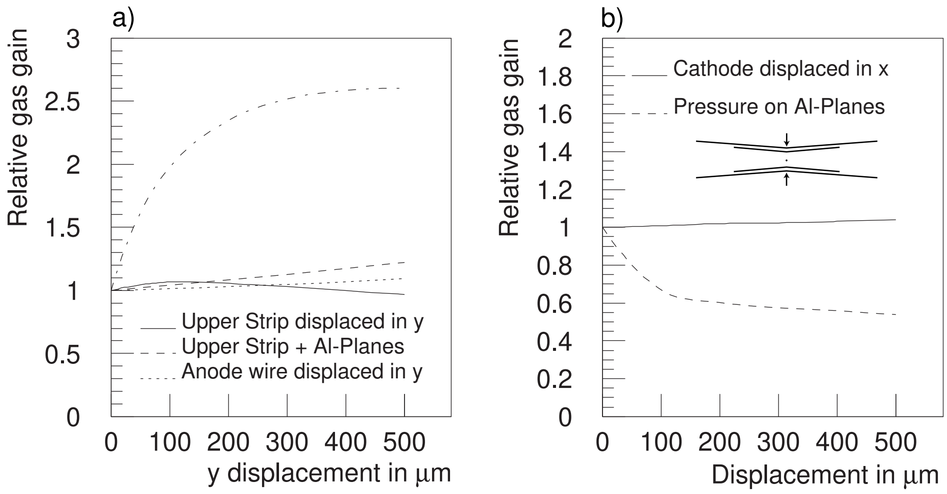
a)
Relative gas gain
3
2.5
2
1.5
1
0.5
0
Upper Strip displaced in y
Upper Strip + Al-Planes
Anode wire displaced in y
0
100
200
300
400
500
y displacement in μm
b)
Relative gas gain
2
1.8
1.6
1.4
1.2
1
0.8
0.6
0.4
0.2
0
Cathode displaced in x
Pressure on Al-Planes
0
100
200
300
400
500
Displacement in μm

Fig. 9.

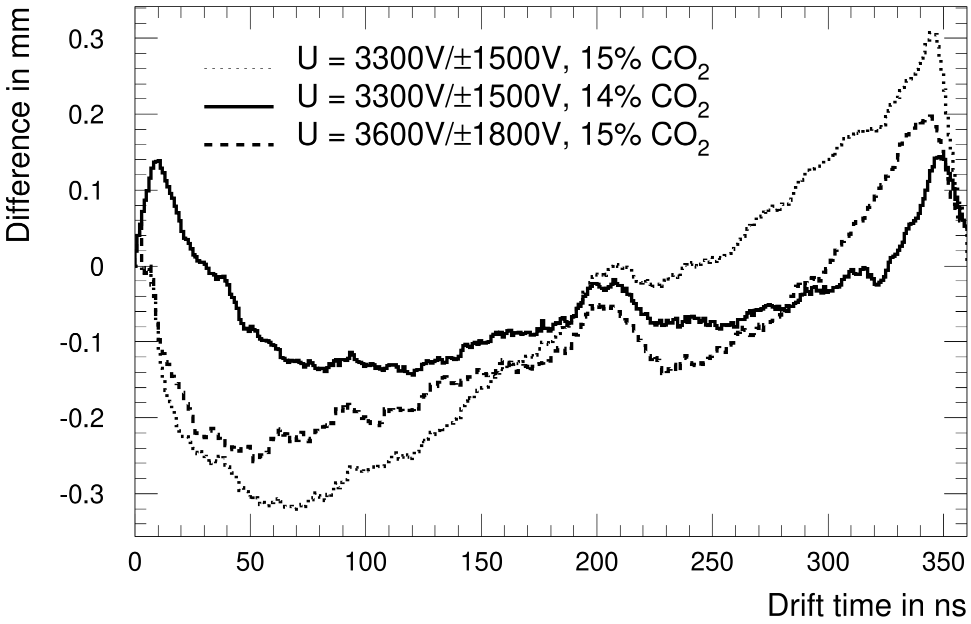

Difference in mm
0.3
0.2
0.1
0
-0.1
-0.2
-0.3
U = 3300V/±1500V, 15% CO2
U = 3300V/±1500V, 14% CO2
U = 3600V/±1800V, 15% CO2
0
50
100
150
200
250
300
350
Drift time in ns

Fig. 10.

Table 1
Single hit resolutions from Simulation in comparison to test beam measurements for three different incidence angles Φ.

Angle Φ in ^{o}	0		10		20	
	Simulation	Data	Simulation	Data	Simulation	Data
Resolution σ_x	$172\,\mu$m	$195\,\mu$m	$191\,\mu$m	$207\,\mu$m	$201\,\mu$m	$215\,\mu$m